

Neutrino diffusive transport in hot quark matter: a detailed analysis

Gustavo C. Colvero and Germán Lugones

*Universidade Federal do ABC, Rua Santa Adélia 166, Santo André, SP, 09210-170, Brazil.**

(Received 17 February 2014; Published)

We perform an extensive analysis of neutrino diffusion in quark matter within the MIT bag model at arbitrary temperature and degeneracy. We examine in detail the contribution of each of the relevant weak interaction processes to the total neutrino opacity and evaluate the effect of the strange quark mass, the bag constant, and the QCD perturbative corrections to the MIT bag model. We also investigate the anisotropic contribution to the neutrino distribution function in scatterings, the mean energy transfer and the mean scattering angle. The density and temperature dependence of the diffusion coefficients D_n that govern the cooling and deleptonization of a compact star is shown in detail. Finally, our numerical results for the neutrino mean free paths are compared against known analytic approximations. We conclude that neutrino scattering constitutes a significant portion of the total neutrino opacity in leptonized quark matter and neutrino-quark scattering is, in general, very similar to neutrino-electron scattering with respect to both mean energy transfer per scattering and mean scattering angle.

PACS numbers: 97.60.Jd, 21.65.Qr, 13.15.+g

I. INTRODUCTION

Compact stellar objects containing deconfined quark matter have been envisaged since long ago [1–5]. According to theoretical studies such objects could be formed if the density inside a purely hadronic star goes beyond a critical density [6]. This may happen due to accretion onto a cold hadronic star in a binary system, as a consequence of cooling, deleptonization and fallback accretion during the proton-neutron star phase of a just born compact star, due to spin down of a fast rotating star or by more exotic mechanisms such as strangelet contamination [7–9]. The conversion of the star presumably begins through the formation of a small quark matter seed that grows at the expenses of the gravitational energy extracted from the contraction of the object and/or through strongly exothermic combustion processes [10–14]. All these scenarios lead to the formation of hot and neutrino rich quark matter occupying the whole compact object (strange star) or its core (hybrid star).

A full comprehension of the above mechanisms requires a detailed knowledge of the neutrino transport in quark matter. In fact, neutrino interactions in neutron star matter have been studied in detail for a long time now. Most of the early contributions were given in the form of approximate treatments focused on a particular state of neutrino degeneracy: neutrinos were considered to be either nondegenerate or highly degenerate. From these works, those which are particularly important for the present analysis have been summarized by Iwamoto [15], with emphasis in neutrino interactions in quark matter.

Extensive numeric analyses for arbitrary temperatures, densities and neutrino level of degeneracy, however, are not so abundant. In this case, we may cite the works of Reddy & Prakash [16] and Reddy, Prakash & Lattimer

[17], where neutrino interactions in hadronic neutron star matter with the possible presence of hyperons have been studied.

Works focused on neutrino interactions in quark matter at arbitrary conditions are even rarer and the reference for this topic is usually the paper of Steiner, Prakash & Lattimer [18]. In that work, the authors analyse the neutrino diffusion coefficients in the interior of a hybrid star containing a mixed quark-hadron phase and quark matter was described using the MIT bag model with a fixed bag constant $B = 200 \text{ MeV/fm}^3$.

In the present work, we intend to fill the gap in the literature represented by the lack of studies exploring general aspects of neutrino interactions and diffusive neutrino transport in quark matter in general conditions. We describe quark matter using the MIT bag model and analyze the influence of its three possible free parameters – the bag constant B , the mass of the strange quark m_s and the strong coupling constant α_c – on the neutrino mean free paths and energy-averaged diffusion coefficients. We pay particular attention to the relative contributions of absorption and scattering to the total neutrino opacity and how neutrino-quark scattering compares to neutrino-electron scattering. Having time-consuming simulations in mind, we explore different expressions for the neutrino scattering opacity and the possible penalties in precision associated to more simplified treatments. We also explore here the actual range of validity of the known analytic approximate forms for the neutrino mean free paths.

II. BOLTZMANN TRANSPORT IN THE DIFFUSIVE REGIME

Neutrino transport is described in terms of the Boltzmann transport equation for massless particles, which dictates the kinetic evolution of its invariant distribution

* gustavo.colvero@gmail.com; german.lugones@ufabc.edu.br

function $f = f(x, p)$:

$$p^\alpha \frac{Df}{dx^\alpha} = \left(\frac{df}{d\tau} \right)_{\text{coll.}}, \quad (1)$$

where, in the general relativistic case, D/dx^α denotes the operator $\partial/\partial x^\alpha - \Gamma_{\alpha\gamma}^\beta p^\gamma \partial/\partial p^\beta$, with $\Gamma_{\alpha\gamma}^\beta$ being the Christoffel symbols. The right-hand side of Eq. (1) designates the changes in f due to particle interaction processes (“collisions”) and it can be separated into different contributions

$$\left(\frac{df}{d\tau} \right)_{\text{coll.}} = B_{\text{AE}}[f] + B_{\text{S}}[f] + \dots, \quad (2)$$

where AE stands for absorption/emission of neutrinos and S designates all forms of scattering. Here, we will focus only on these two kind of processes, since those are the dominant ones on neutron star matter at the typical values of temperature and lepton degeneracy we are interested in. For processes of the form $\nu + 2 \rightarrow 3 + 4$, each contribution to Eq. (2) can be explicitly written in the generic “collision integral”

$$B[f] = - \int \frac{d^3 p_2}{(2\pi)^3} \int \frac{d^3 p_3}{(2\pi)^3} \int \frac{d^3 p_4}{(2\pi)^3} \left\{ \begin{aligned} &\times g_\nu g_2 f(E_\nu) f_2(E_2) [1 - f_3(E_3)] [1 - f_4(E_4)] W_{fi} \\ &- g_3 g_4 [1 - f(E_\nu)] [1 - f_2(E_2)] f_3(E_3) f_4(E_4) W_{if} \end{aligned} \right\} \quad (3)$$

where f_i denotes the distribution function for particle species i , f is the complete neutrino distribution function and the g_i denote the phase-space spin degeneracy for each particle. Here, W_{fi} represents the transition rate between the initial and the final states for the given process. We can define the neutrino emissivity j_a and the absorptivity $1/\lambda_a$ through

$$B_{\text{AE}}[f] = [1 - f(E_\nu)] j_a - \frac{f(E_\nu)}{\lambda_a}, \quad (4)$$

and the scattering contribution to the collision integral can be written as

$$B_{\text{S}}[f] = [1 - f(E_\nu)] \int \frac{d^3 p_4}{(2\pi)^3} f(E'_\nu) R^{in} - f(E_\nu) \int \frac{d^3 p_4}{(2\pi)^3} [1 - f(E'_\nu)] R^{out}, \quad (5)$$

where $R^{in/out}(E_\nu, E'_\nu, \cos\theta)$ are the scattering kernels, θ being the scattering angle. When the pairs of reactions of emission/absorption and scattering in/out are balanced, the transition rates satisfy the reciprocity relations $g_\nu g_2 W_{if} = g_3 g_4 W_{fi}$ and we have the relations of detailed balance

$$\frac{1}{\lambda_a} = e^{(E_\nu - \mu_\nu)/T} j_a, \quad R^{in} = e^{(E'_\nu - E_\nu)/T} R^{out}, \quad (6)$$

i.e., Eqs. (4) and (5) have only one independent contribution each.

The *diffusive approximation* consists of assuming that matter is at thermodynamic equilibrium and neutrinos are only slightly out of equilibrium. Since the equilibrium states of our MIT bag model are those of a gas non-interacting fermions, we automatically set each f_i in Eq. (3) to the corresponding Fermi-Dirac distribution function, f_0 . On this regime, neutrinos are expected to *relax* in a very short time scale and their distribution function differs from its equilibrium value only by a small anisotropic factor. In terms of a Legendre expansion of f , the diffusion approximation can be written as

$$f(E_\nu) \simeq f_0(E_\nu) + \mu f_1(E_\nu), \quad (7)$$

where μ is the cosine of the angle between the neutrino propagation direction and the radial vector, and $|f_1(E_\nu)| \ll 1$.

All the quantities we are interested in in the study of neutrino transport will be defined in terms of f and its angular moments of the form $\frac{1}{2} \int_{-1}^1 d\mu \mu^i f$ [19–21]. With the use of the approximation given by Eq. (7), it is possible to write the angular moments of Eq. (2) in a very convenient form. The 0-th moment will be associated with neutrino source terms [21] and, since we are assuming the detailed balance of Eqs. (6), it is identically zero. The 1st moment, on the other hand, contains the traditional *opacities* and it is given by

$$\frac{1}{2} \int_{-1}^1 \mu B[f] d\mu = - \frac{f_1(E_\nu)}{3} \left(j_a + \frac{1}{\lambda_a} + \kappa_1 \right), \quad (8)$$

where

$$\kappa_1 = \frac{1}{(2\pi)^2} \int_0^\infty dE'_\nu E'^2_\nu \left\{ \frac{[1 - f_0(E'_\nu)]}{[1 - f_0(E_\nu)]} R_0^{out} - \frac{f_0(E_\nu) f_1(E'_\nu)}{f_1(E_\nu) f_0(E'_\nu)} R_1^{out} \right\}. \quad (9)$$

We have defined here the Legendre moments of the scattering kernel in terms of the scattering angle θ

$$R_l^{out} = \int_{-1}^1 d\cos\theta P_l(\cos\theta) R^{out}(E_\nu, E'_\nu, \cos\theta), \quad (10)$$

with $\cos\theta = \mu\mu' + \sqrt{(1 - \mu^2)(1 - \mu'^2)} \cos\phi$, where ϕ is the azimuthal angle of one neutrino with respect to each other.

The first term between the curly braces in Eq. (9) gives the inverse neutrino scattering mean free path when neutrinos are in thermodynamic equilibrium with the rest of the matter, and we denote it here by $1/\lambda_s$:

$$\frac{1}{\lambda_s} = \frac{[1 - f_0(E_\nu)]^{-1}}{(2\pi)^2} \int_0^\infty dE'_\nu E'^2_\nu [1 - f_0(E'_\nu)] \times \int_{-1}^1 d\cos\theta R^{out}(E_\nu, E'_\nu, \cos\theta). \quad (11)$$

Eq. (11) is just Eq. (3) with f_0 for the neutrino distribution function and it can be written without one explicitly defining the scattering kernel R^{out} .

When the scattering process is isoenergetic (meaning that neutrinos and matter do not exchange energy), regardless the actual neutrino distribution function, Eq. (9) specializes to

$$\kappa_1^{\text{is}} = \frac{E_\nu^2}{(2\pi)^2} \int_{-1}^1 d\cos\theta \times (1 - \cos\theta) R^{\text{out}}(E_\nu, E_\nu, \cos\theta), \quad (12)$$

which is a common form of scattering opacity used in different applications. In a general situation, however, κ_1 depends explicitly on f_1 , which is, *a priori* unknown.

From the energy-dependent diffusion coefficient $D(E_\nu) = (j_a + 1/\lambda_a + \kappa_1)^{-1}$, we define the energy-averaged coefficients [21]

$$D_n = \int_0^\infty dx x^n f_0(E_\nu) [1 - f_0(E_\nu)] D(E_\nu), \quad (13)$$

where $x = E_\nu/T$. In particular, the Rosseland energy-averaged neutrino mean free path [17, 22] can be defined as

$$\lambda_R = \frac{D_4}{\int_0^\infty dx x^4 f_0(E_\nu) [1 - f_0(E_\nu)]}. \quad (14)$$

III. NEUTRINO INTERACTIONS

All neutrino processes under consideration are listed on Table I. Electron neutrino absorption on quarks d and s involve the exchange of a W boson, while neutrino scattering on quarks or on leptons may involve either the exchange of W or Z bosons. At the energy density regime we are interested in, the neutrino energy is always much smaller than the W and Z masses and the interactions may be described in terms of current-current couplings [15, 17, 23]. Weak charged currents are associated to both neutrino absorption and neutrino scattering on leptons of the same generation, while weak neutral currents take part in neutrino scattering on either leptons or quarks. Given that it is possible to write the charged current contribution of a scattering process in terms of a neutral current (and vice-versa), we may write the current-current interaction Lagrangian in a combined form as

$$\mathcal{L}_{\text{int}} = \frac{G_F}{\sqrt{2}} [\bar{u}(\nu)\gamma_\mu(1 - \gamma_5)u(4)] \times [\bar{u}(2)\gamma^\mu(C_A - C_V\gamma_5)u(3)] + \text{H.C.}, \quad (15)$$

with C_A and C_V being the appropriate axial and vector coupling constants to be read from Table I and G_F is the Fermi weak coupling constant ($G_F/c\hbar^3 = 1.664 \times 10^{-5} \text{GeV}^{-2}$).

The transition rates W_{if} appearing in Eq. (3) are obtained from the matrix element by means of Femi's golden rule:

$$W_{if} = (2\pi)^4 \delta^4(p_\nu + p_2 - p_3 - p_4) \frac{\langle |\mathcal{M}|^2 \rangle}{2^4 E_\nu E_2 E_3 E_4}, \quad (16)$$

TABLE I. Vector and axial vector coupling constants for the charged and neutral currents under consideration. We use the values $\cos\theta_C = 0.973$ and $\sin^2\theta_W = 0.231$. The corresponding scattering of antineutrinos involves only the substitution $C_A \rightarrow -C_A$.

| $\nu + 2 \rightarrow 3 + 4$ | C_V | C_A |
|---|--|-----------------|
| $\nu_e + d \rightarrow u + e^-$ | $\cos\theta_C$ | $\cos\theta_C$ |
| $\nu_e + s \rightarrow u + e^-$ | $\sin\theta_C$ | $\sin\theta_C$ |
| $\bar{\nu}_e + u \rightarrow d + e^+$ | $\cos\theta_C$ | $-\cos\theta_C$ |
| $\bar{\nu}_e + u \rightarrow s + e^+$ | $\sin\theta_C$ | $-\sin\theta_C$ |
| $\nu_l + u \rightarrow u + \nu_l$ | $\frac{1}{2} - \frac{4}{3}\sin^2\theta_W$ | $\frac{1}{2}$ |
| $\nu_l + d \rightarrow d + \nu_l$ | $-\frac{1}{2} + \frac{2}{3}\sin^2\theta_W$ | $-\frac{1}{2}$ |
| $\nu_l + s \rightarrow s + \nu_l$ | $-\frac{1}{2} + \frac{2}{3}\sin^2\theta_W$ | $-\frac{1}{2}$ |
| $\nu_e + e^- \rightarrow e^- + \nu_e$ | $\frac{1}{2} + 2\sin^2\theta_W$ | $\frac{1}{2}$ |
| $\nu_{\mu,\tau} + e^- \rightarrow e^- + \nu_{\mu,\tau}$ | $-\frac{1}{2} + 2\sin^2\theta_W$ | $-\frac{1}{2}$ |

where $\langle |\mathcal{M}|^2 \rangle$ denotes the squared matrix element summed over final spins and averaged over the initial spins. From Eq. (15) we may then derive an expression for W_{if} also valid for both absorption and scattering processes:

$$W_{fi} = \frac{G_F^2}{E_\nu E_2 E_3 E_4} [(C_V + C_A)^2 (p_\nu \cdot p_2)(p_3 \cdot p_4) + (C_V - C_A)^2 (p_\nu \cdot p_3)(p_2 \cdot p_4) - (C_V^2 - C_A^2) m_2 m_3 (p_\nu \cdot p_4)] \times (2\pi)^4 \delta^4(p_\nu + p_2 - p_3 - p_4), \quad (17)$$

where m_i is the mass of the corresponding particle.

The explicit form of the expressions used for the inverse mean free paths and for the scattering kernels can be found on appendices A and B, respectively.

IV. QUARK MATTER EQUATION OF STATE

We describe quark matter constituted of u , d and s quarks, plus electrons and electron-neutrinos in terms of the MIT bag model [24]. The thermodynamics follows from the Grand potential (per unit volume)

$$\Omega = \sum_{i=u,d,s,e,\nu} \Omega_i, \quad (18)$$

where Ω_i is the thermodynamic potential for a gas of ideal fermions

$$\Omega_i(T, \mu_i) = -\frac{g_i T}{2\pi^2} \int dk k^2 \ln \left[1 + e^{-(E_k - \mu_i)/T} \right]. \quad (19)$$

Antiparticles are included through $\Omega_i(T, -\mu_i)$ and all derived thermodynamic quantities must be understood as net quantities, containing the contributions of both particles and antiparticles.

The inclusion of the vacuum energy density B (the bag constant), requires that both the pressure and energy density are modified according to

$$P = -\Omega - B, \quad (20)$$

$$\rho = \Omega + \sum_i (Ts_i + \mu_i n_i) + B, \quad (21)$$

where the entropy density, s_i , and the particle number densities, n_i , are derived from Ω by the usual thermodynamic relations.

The five chemical potentials ($\mu_u, \mu_d, \mu_s, \mu_e, \mu_{\nu_e}$) at given temperature, baryon number density, $n_B = (n_u + n_d + n_s)/3$, and fixed net electron-type lepton fraction, $Y_L = (n_e + n_{\nu_e})/n_B$, are determined by means of the conditions of β -equilibrium

$$\mu_d = \mu_u + \mu_e - \mu_{\nu_e}, \quad (22)$$

$$\mu_s = \mu_d, \quad (23)$$

and electric charge neutrality

$$n_e = \frac{2}{3}n_u - \frac{1}{3}(n_d + n_s). \quad (24)$$

When quark matter doesn't have trapped neutrinos, or when the trapped neutrinos are nondegenerate, the electron chemical potential is always much smaller than those of quarks. Quark matter in these circumstances requires only a small fraction of electrons to be electrically neutral. When the rate of occurrence of the weak interaction processes is high enough for neutrinos to become trapped and degenerate in quark matter, an increase in the abundance of electrons follows, as it can be seen from the behavior of the electron chemical potential in Fig. 1. In fact, as shown in Fig. 1, the degeneracy of electrons in quark matter follows closely that of neutrinos. This moderate uniformity between the electron and electron-neutrino chemical potentials, allows us to use the total electron-type lepton fraction Y_L as an indicative of both the electron and electron-neutrino state of degeneracy, as we show in Fig. 2.

QCD corrections to the thermodynamic potential of Eq. (19) for arbitrary temperatures, quark masses and chemical potentials have been derived for the orders of α_c and $\alpha_c^{3/2}$ in perturbation theory [25]. Closed-form expressions are known only on the approximate regimes. For degenerate massless quarks, one has, to first order in $\alpha_c = g^2/4\pi$ [26]

$$\Omega_{(2)} = \sum_{f=u,d,s} \left[\frac{7}{60} \pi^2 T^4 \left(\frac{50}{21} \frac{\alpha_c}{\pi} \right) + \left(\frac{1}{4\pi^2} \mu_f^4 + \frac{1}{2} T^2 \mu_f^2 \right) \left(2 \frac{\alpha_c}{\pi} \right) \right], \quad (25)$$

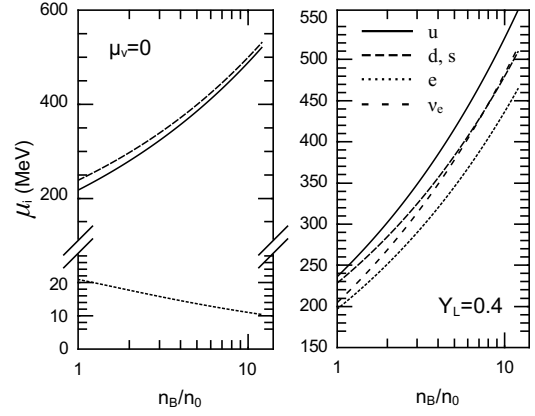


FIG. 1. Equilibrium chemical potentials of quark matter constituted only of the three lightest quarks at $T = 30\text{MeV}$ as a function of the baryon number density. The panel at the left corresponds to neutrino-free quark matter. The panel at the right represents quark matter with trapped neutrinos, corresponding to a total electron-type lepton fraction of $Y_L = 0.4$. For this figure, $B = 60\text{MeV}/\text{fm}^3$ and $m_s = 150\text{MeV}$.

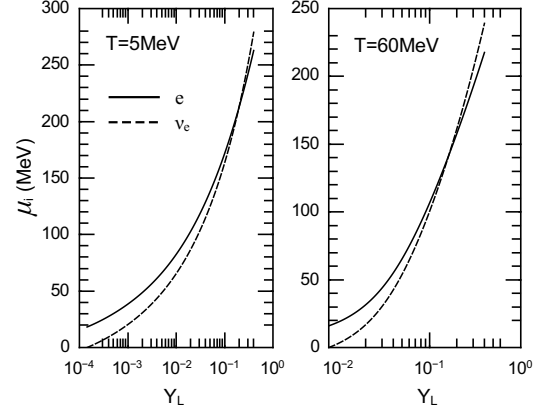


FIG. 2. Electron and electron-neutrino equilibrium chemical potentials in quark matter with trapped neutrinos at $n_B = 2n_0$ for two different temperatures. The smallest value of Y_L shown in this figure always represent neutrino-free quark matter, for which $Y_L = Y_e$. The largest value of Y_L has been chosen to be $Y_L = 0.4$ in both panels. Note how an increasing neutrino degeneracy is followed by an increasing electron degeneracy for fixed temperature and baryon density. For this figure, $B = 60\text{MeV}/\text{fm}^3$ and $m_s = 150\text{MeV}$.

and the thermodynamic potential to second order is obtained through $\Omega \rightarrow \Omega + \Omega_{(2)}$. In the context of the MIT bag model, the strong coupling constant, α_c , is regarded as a numeric constant. Together, B , m_s and α_c constitute the three free parameters of the model.

Throughout this paper we use mainly the set of parameters $B = 60\text{MeV}/\text{fm}^3$, $m_s = 150\text{ MeV}$ and $\alpha_c = 0$, which falls inside the stability window of Ref. [24] and, consequently, describes absolutely stable (strange) quark matter, with an energy per baryon at zero pressure and temperature smaller than the neutron's mass. However,

we employ also other parameter sets, some of which represent standard (non-absolutely stable) quark matter. In particular, at the end of Sec. V A, we show how each of B , m_s and α_c affect the neutrino mean free paths through their influence on the equilibrium chemical potentials.

V. RESULTS

A. Neutrino inverse mean free paths and diffusion coefficients

Our results are shown separately in terms of either nondegenerate or highly degenerate neutrinos. To non-degenerate neutrinos we associate a chemical potential $\mu_\nu = 0$. Degenerate neutrinos, on the other hand, must have $\mu_\nu \gg T$. We represent the latter category in terms of a high net electron-neutrino lepton fraction $Y_L = (n_e + n_{\nu_e})/n_B$, where n_e and n_{ν_e} represent, respectively, electron and electron-neutrino net number densities (number density of particles minus number density of the corresponding antiparticles) and n_B is the baryon number density.

In Fig. 3 we show the inverse neutrino mean free paths associated to the six electron-neutrino processes listed in Table I. It must be noted that the factor $[1 - f_0(E_\nu)]^{-1}$ present in Eq. (11) has been kept so the curves can be better distinguished in the region $E_\nu < T$.

When neutrinos are nondegenerate, neutrino-quark scattering dominates the scattering opacity with respect to neutrino-electron scattering by orders of magnitude. This discrepancy can be explained by the tiny density of electrons present in quark matter. The presence of trapped degenerate neutrinos also increases the electron density and hence the neutrino-electron contribution to the scattering opacity also increases, as can be seen in the lower panel at the left. In both the upper and the lower panels at the left in Fig. 3, it can be seen that neutrino-strange quark scattering differs from the other scatterings mainly at lower neutrino energies. In the panels at the right in Fig. 3 we show the neutrino inverse mean free paths associated with absorption. In general, the process of neutrino absorption on d quarks dominates the opacity. The contribution of neutrino absorption on s quarks, on the other hand, tends to be smaller than that of scatterings, with exception of the very low neutrino energy regime, in which this process dominates the opacity. These results are in agreement with the results found in Ref. [18].

The behavior of the neutrino inverse mean free paths with respect to baryon number density for fixed neutrino energies is shown in Figs. 4 and 5. It can be seen that the contribution of neutrino-electron scattering is always small in comparison with that of neutrino-quark scattering when neutrinos are nondegenerate. It is only when neutrinos are trapped and highly degenerate, implying in an also higher abundance of electrons, that neutrino-electron scattering becomes an important contribution to

the total opacity, as it is shown in the lower panels of Fig. 5. It is noticed that, for fixed T , the inverse mean free paths vary within one order of magnitude in the baryon number density range of interest. In contrast, the temperature dependence is stronger, e.g. there is a variation of more than two orders of magnitude when T goes from 5 MeV to a value above 30 MeV.

The combined scattering processes amount to at least 10% of the total Rosseland mean free path, as shown in Fig. 6. In the case of leptonzied quark matter, neutrino scattering represents $\sim 40\%$ of the total neutrino opacity. It is only when neutrinos are less degenerate in colder quark matter that neutrino absorption becomes dominant. Even in this case, as we already mentioned, neutrino scattering will contribute to at least $\sim 10\%$ of the total opacity in lower density regions of the star where neutrinos are completely nondegenerate.

In Figs. 7 and 8 we show the diffusion coefficients D_2 , D_3 and D_4 for both electron-neutrinos and electron-antineutrinos. When neutrinos are nondegenerate, all diffusion coefficients decrease with increasing density. As it can be seen in the panels at the middle, the combined coefficient $D_3 = D_{3,\nu_e} - D_{3,\bar{\nu}_e}$ will be negative. In Fig. 8 it can be seen that the behavior of D_2 , D_3 and D_4 for degenerate neutrinos is not the same with respect to increasing density. Notoriously, D_2 decreases, while D_4 increases. This behavior can be anticipated by means of analytic approximations for degenerate neutrinos, as we show in Appendix D.

In Figs. 9 through 11 we analyze separately how m_s , B and α_c indirectly influence the neutrino Rosseland mean opacity through their effects on the equilibrium composition of quark matter as a function of pressure for a given temperature. In Eq. (20), it is seen that, for a given P , a larger B will imply in a larger absolute value of Ω . For fixed m_s and α_c , it follows that the equilibrium chemical potentials will increase accordingly. As verified in Fig. 9, this implies in smaller mean free paths. From Eq. (25), it follows that the same reasoning applies for increases in α_c and this is shown in Fig. 10. For last, we analyze the influence of the strange quark mass on the neutrino mean free paths. Since m_s enters not only in the equation of state but also directly in the computation of the mean free paths in a nontrivial way, its influence is inferred directly from the numeric results shown in Fig. 11, where it can be seen that an increase in m_s leads to larger mean free paths.

It follows then that increases in both B and α_c lead to decreases in the neutrino mean free paths. The effect of increasing α_c , however, is distinct from that of increasing B in the sense that its effect is more prominent at higher pressures. It can also be noted that the mean free paths of highly degenerate neutrinos in highly degenerate quark matter is less sensitive to changes in m_s or α_c , since in these situations the chemical potentials are already very high.

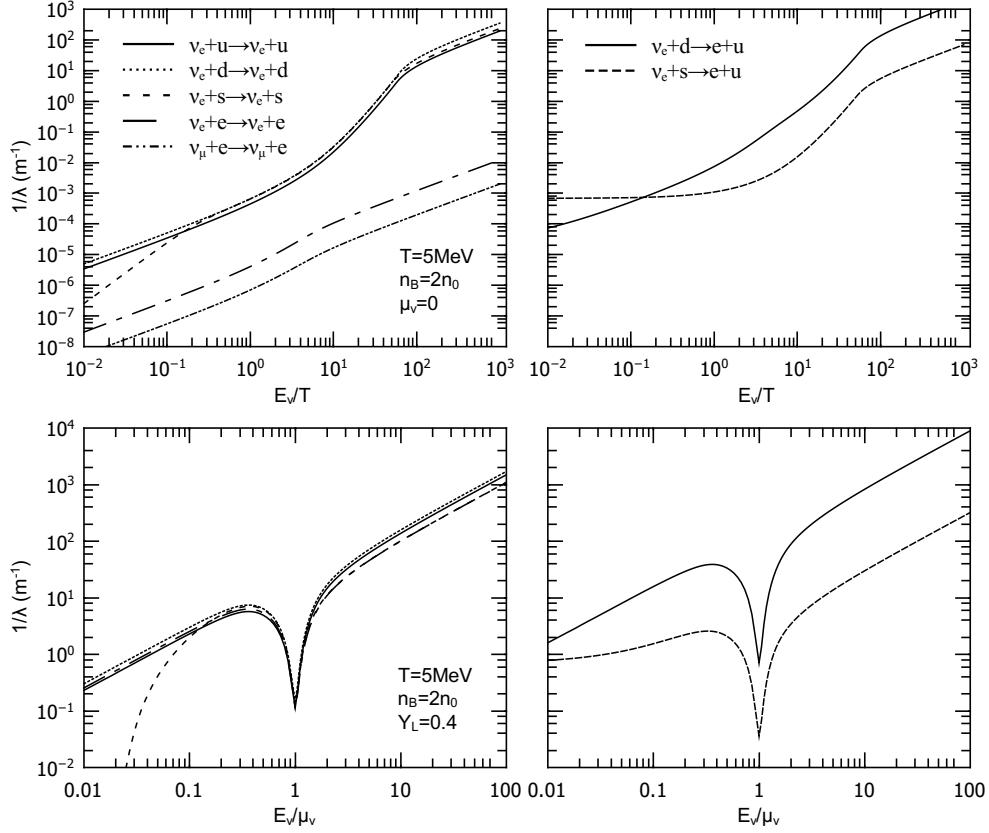


FIG. 3. Inverse neutrino mean free paths, Eq. (A1), in quark matter at two times nuclear saturation density and $T = 5\text{MeV}$. At the upper panels, we have $\mu_{\nu_e} = 0$ representing nondegenerate neutrinos. At the left, we have included muon neutrino-electron scattering for comparison. At the lower panels, $Y_L = 0.4$ represents highly degenerate neutrinos and matter. Results for degenerate neutrinos have been divided by $[1 - f_0(E_\nu)]$, so the curves can be better seen in the range $E_\nu < \mu_\nu$.

B. Error estimate associated with the disregard of the anisotropic contribution to the neutrino distribution function in scatterings

We have seen that scattering may represent a considerable fraction of the total neutrino opacity in quark matter. It is evident then that neutrino scattering must be treated with proper care. Now we wish derive an estimate of the error committed when the term containing f_1 in Eq. (9) is neglected and Eq. (11) is used as the neutrino inverse scattering mean free path. Even though we do not know an explicit form for f_1 , it is expected to be much smaller than f_0 in magnitude on the regions of higher density, where we expect neutrinos to be almost in thermodynamic equilibrium with the remaining of the matter. In this case, the ratio λ_s^{-1}/κ_1 tends to unity, given that the term containing f_1 in Eq. (9) becomes vanishingly small compared to the first term and Eq. (9) tends to Eq. (11). On the other hand, on the regions of extremely small neutrino opacity, neutrinos will stream almost freely and, in the limit of free stream, $f_1(E_\nu) \sim 3f_0(E_\nu)$ and the ratio λ_s^{-1}/κ_1 deviates maximally from the unity.

A fairly general expression relating f_1 and f_0 on the

surface of a stellar core may be written in the form [19]

$$f_1(E_\nu) = K f_0(E_\nu), \quad (26)$$

where K is responsible for smoothly shifting the neutrino flux from isotropic to radially outward as the optical depth increases. In fact, as the optical depth becomes larger, Eq. (26) will hold not only on the stellar surface but in a whole thick layer where neutrinos stream freely. In principle, K should depend on the neutrino energy, however, to avoid further complications we consider it as a constant geometric factor. In this case, Eq. (9) reduces to

$$\begin{aligned} \kappa_1^{\text{free}} &= \frac{1}{\lambda_s} - \frac{1}{(2\pi)^2} \int_0^\infty dE'_\nu E_\nu'^2 \int_{-1}^1 d\cos\theta \cos\theta R^{\text{out}} \\ &= \frac{1}{\lambda_s} - \frac{1}{(2\pi)^2} \int_0^\infty dE'_\nu E_\nu'^2 R_1^{\text{out}}(E_\nu, E'_\nu), \end{aligned} \quad (27)$$

and the ratio $\lambda_s^{-1}/\kappa_1^{\text{free}}$ represents a bound to the maximum deviation from unity possible. In other words, the ratio λ_s^{-1}/κ_1 will always be closer to 1 than it is $\lambda_s^{-1}/\kappa_1^{\text{free}}$. This information can be used as an estimate of the largest possible error committed on the computation of the scattering contribution to the opacity when λ_s^{-1} is used in the place of κ_1 .

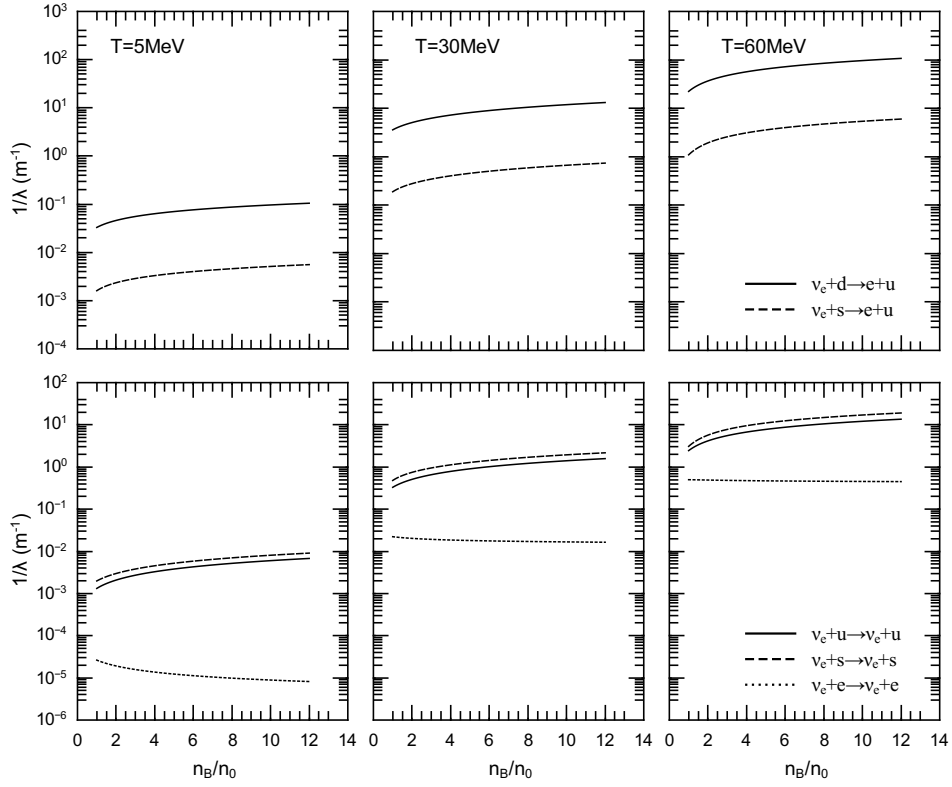


FIG. 4. Inverse mean free paths of nondegenerate neutrinos ($\mu_\nu = 0$) in quark matter as a function of baryon density. On this figure, $E_\nu = 3T$. In the lower panels, neutrino-down quark scattering was omitted since the corresponding curve superposes that of neutrino-strange quark scattering.

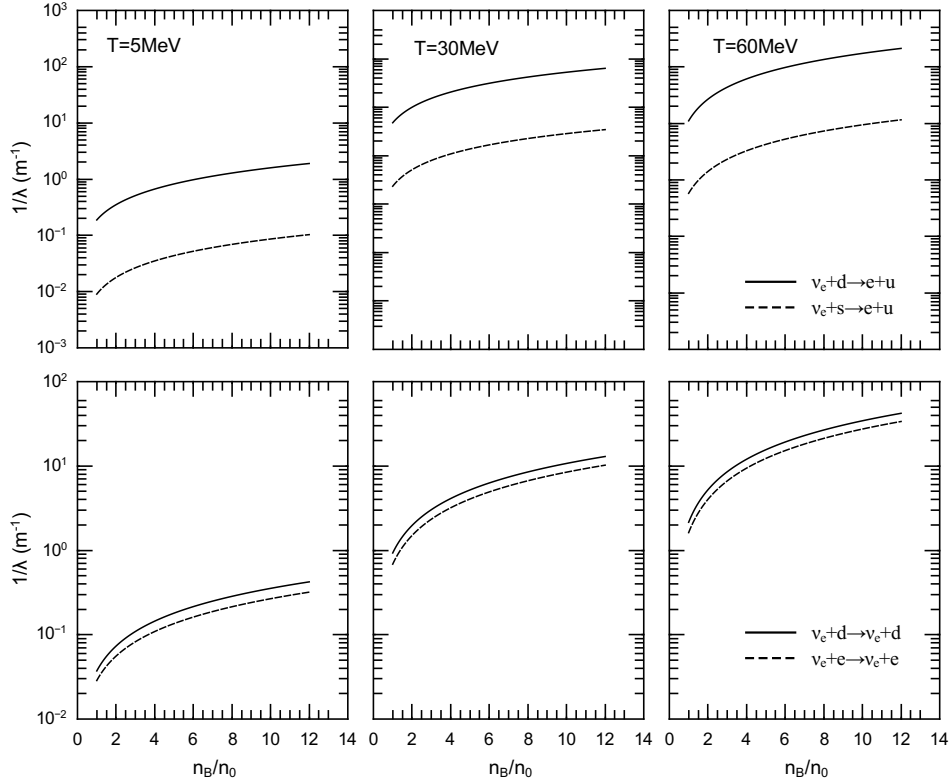


FIG. 5. Inverse mean free paths of degenerate neutrinos ($Y_L = 0.4$) in quark matter as a function of baryon density. For this figure, $E_\nu = \mu_\nu$. The curves associated to neutrino scattering on u and s quarks lie between the curves shown in the lower panels and have been omitted.

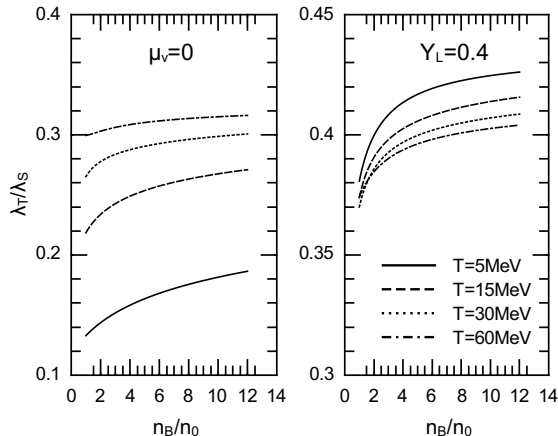


FIG. 6. Scattering contribution to the total Rosseland mean free path as a function of baryon density at several temperatures for both nondegenerate and degenerate neutrinos. All electron-neutrino processes of Table I have been included in the total opacity.

When neutrinos are nondegenerate, it can be seen in Fig. 12 that which between λ_s^{-1} and κ_1^{free} is greater depends on the incident neutrino energy. For $E_\nu < T$, λ_s^{-1} tends to be $\sim 20\%$ smaller than κ_1^{free} . For $E_\nu \gg T$, we see that the contribution of the term containing R_1^{out} in Eq. (27) becomes larger and κ_1^{free} becomes many times smaller than λ_s^{-1} as the energy of the incident neutrino increases. In Fig. 13 we see that when neutrinos are degenerate, there's almost no distinction between the two calculated scattering opacities when $E_\nu \ll \mu_\nu$. However, for neutrinos with $E_\nu \simeq \mu_\nu$, there is a noticeable difference, that increases with increasing neutrino degeneracy. For instance, when $T = 5\text{MeV}$, λ_s^{-1} is $\sim 30\%$ smaller than κ_1^{free} for $Y_L = 0.4$. For higher neutrino energies with respect to μ_ν , λ_s^{-1} becomes several times greater than κ_1^{free} , similarly to what happens when neutrinos are nondegenerate.

In diffusive transport schemes, one is generally interested in the energy-averaged diffusion coefficients as in Eqs. (13) and (14), whose integrands are weighted with the factor $f_0(1 - f_0)$, which quickly cuts off the higher energies, and features a peak centered at $E_\nu = \mu_\nu$ when neutrinos are degenerate. It means that in practice, λ_s^{-1} will give scattering opacities at most $\sim 20\%$ smaller than the ones that would be obtained if κ_1 was used. We have seen that the scattering contribution to the total Rosseland mean opacity is in the range $10 - 30\%$ for temperatures in the range $5 - 60\text{MeV}$ when neutrinos are nondegenerate (Fig. 6). It follows then that the error committed in the total neutrino opacity, may be estimated to have an upper bound in the range $2 - 6\%$. In regions where neutrinos are very close to thermodynamic equilibrium, and the anisotropy in the neutrino distribution function is vanishingly small, this error is expected to be much smaller.

The situation is very similar when neutrinos are degenerate. In this case, the largest errors will be associated to those shown in Fig. 13 for $E_\nu \simeq \mu_\nu$, which we see to be of about 30% when $T = 5\text{MeV}$ and smaller for larger temperatures. In this case, neutrino scattering amounts to about 40% of the total neutrino opacity (Fig. 6) and the error committed may be estimated to have an upper bound in the range $12 - 4\%$ for temperatures increasing in the range $T = 5 - 60\text{MeV}$. If neutrinos are not expected to be too strongly degenerate in quark matter with temperatures as low as 5MeV , then in this case the estimated upper bound for the error will be closer to 4% .

C. Mean energy transfer and mean scattering angle

Neutrino-electron scattering has long been known to be an important thermalizing agent in neutron star matter [23, 27], while neutrino-baryon scattering is usually regarded as an isoenergetic process [19, 21]. In Ref. [16], Prakash & Lattimer work in detail neutrino scattering in neutron star matter with and without hyperons, nevertheless, no attention has been paid to the aspects of neutrino/matter energy exchange or neutrino mean scattering angles.

A detailed analysis of neutrino scattering in quark matter, however, is missing in the literature. Given that quarks are very degenerate in quark matter and considering, for instance, the large mass of the strange quark with respect to that of electrons, it remains the question of whether neutrino-quark scattering is similar to neutrino-baryon or to neutrino-electron scattering with respect to neutrino-matter energy transfer and mean scattering angles. In this section we show that neutrino-quark scattering is always similar to neutrino-electron scattering with respect to energy exchange and hence non-isoenergetic. Both the mean energy transfer and the mean scattering angle are defined in Appendix C.

The first thing to be noticed in Figs. 14 and 15, is that neutrino-matter energy exchange vanishes on average for a particular incident neutrino energy, E_0 , depending on both the neutrino and matter state of degeneracy. For $E_\nu < E_0$, neutrinos tend to gain energy on average, while for $E_\nu > E_0$, they tend to lose energy. This is not to say that neutrinos with $E_\nu = E_0$ don't exchange energy with matter, but rather, that the net energy exchange vanishes on average. We see that the energy-exchange in neutrino-strange quark scattering is very similar to that in neutrino-electron scattering. The curves representing neutrino-up quark and neutrino-down quark scattering have been omitted since the difference between those and that of neutrino-electron scattering would be barely visible.

When neutrinos are nondegenerate, E_0 lies between $4T$ and $5T$. When neutrinos are degenerate, E_0 lies between μ_ν and $6T$. The exact value depends on the state of degeneracy of the matter, which determines both the mean energy of the particles participating on the reaction

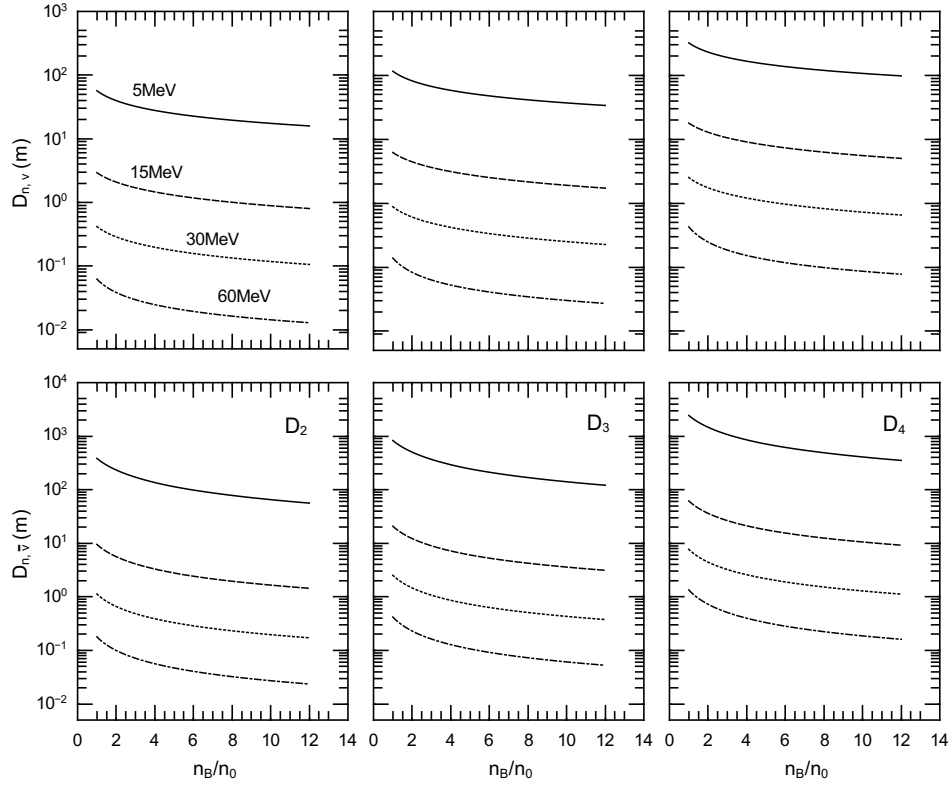


FIG. 7. Diffusion coefficients vs baryon density for nondegenerate ($\mu_\nu = 0$) electron-neutrinos (upper panels) and antineutrinos (lower panels) at different temperatures. The temperatures indicated in panel at the top left are the same for all the other panels.

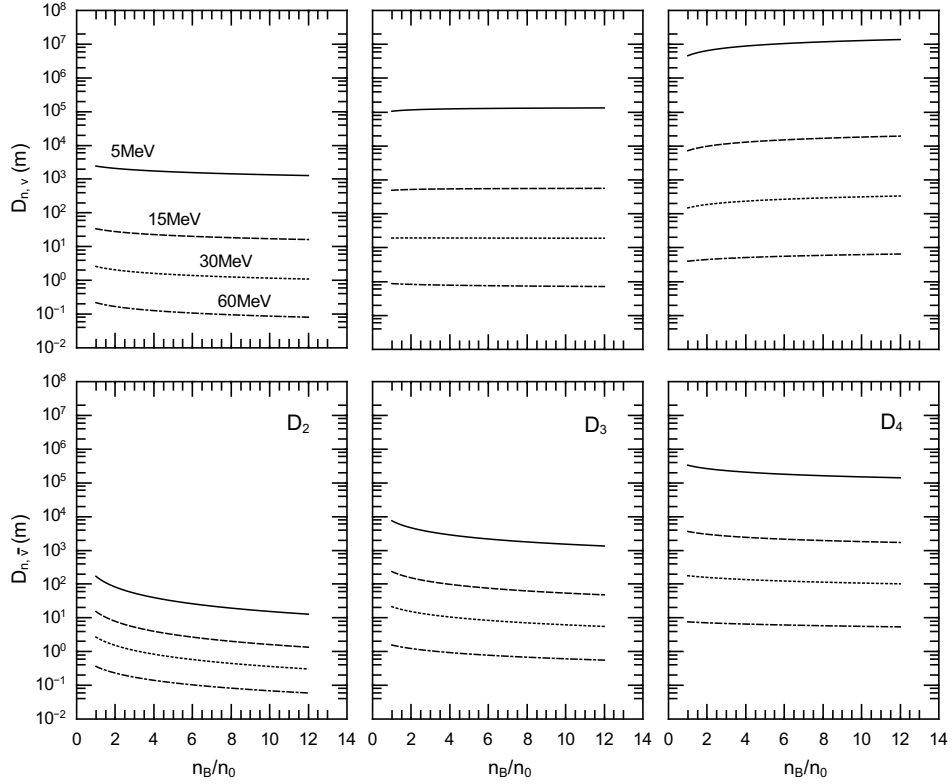


FIG. 8. Diffusion coefficients vs baryon density for degenerate ($Y_L = 0.4$) electron-neutrinos (upper panels) and antineutrinos (lower panels) at different temperatures. The temperatures indicated in panel at the top left are the same for all the other panels.

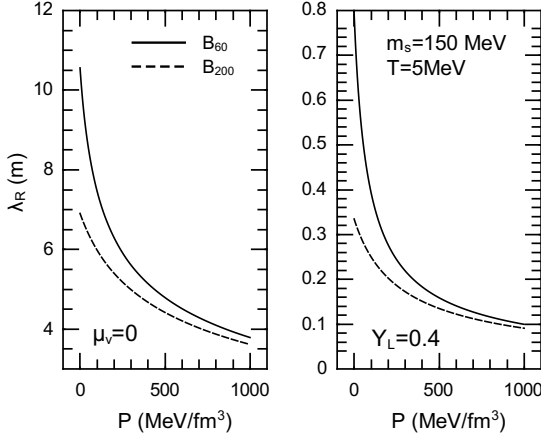


FIG. 9. Influence of the bag constant, B , on the total Rosseland neutrino mean free path of degenerate neutrinos ($Y_L = 0.4$) in quark matter. Here, B_{60} and B_{200} represent $B = 60 \text{ MeV/fm}^3$ and $B = 200 \text{ MeV/fm}^3$, respectively.

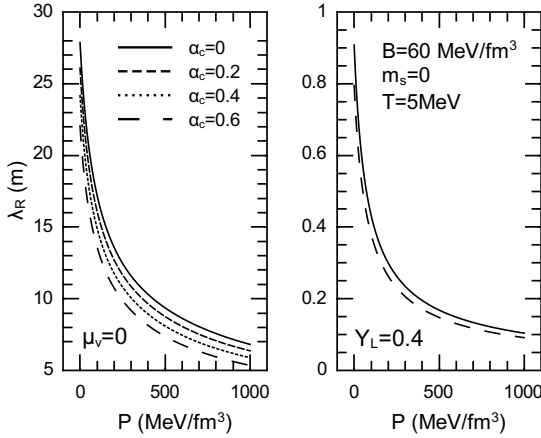


FIG. 10. Influence of the strong coupling constant, α_c , on the total Rosseland neutrino mean free path of nondegenerate (left panel) and of degenerate neutrinos (right panel, $Y_L = 0.4$) in quark matter. In the panel at the right, only the cases $\alpha_c = 0$ and $\alpha_c = 0.6$ are considered. The curves corresponding to $\alpha_c = 0.2$ and $\alpha_c = 0.4$ lie between the two curves shown and have been omitted for clarity purposes.

and the phase space available for the scattered particles [23, 27, 28].

Regardless of the neutrino/matter particular state of degeneracy, it is a general result that highly energetic neutrinos ($E_\nu \gg E_0$) will lose on average half their initial energy in each scattering process, a result previously known for the case of neutrino-electron scattering when neutrinos are nondegenerate [23, 29], and which we extend here for degenerate neutrinos as well. On the other hand, very low-energetic neutrinos can gain on average several times their initial energy in a given scattering process and it is in this energy regime that neutrino-strange quark and neutrino-electron scatterings differ. It can be seen that low-energetic neutrinos tend to gain more en-

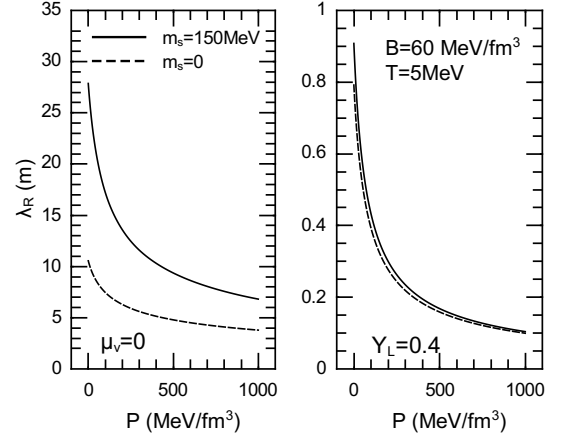


FIG. 11. Influence of the strange quark mass, m_s , on the total Rosseland neutrino mean free path of nondegenerate neutrinos in quark matter with $B = 60 \text{ MeV/fm}^3$.

ergy from electrons (and from up and down quarks) than from strange quarks.

Figs. 16 and 17 show the neutrino mean scattering angle. Less energetic neutrinos will scatter on average by an angle of about 120 degrees. In association with Figs. 14 and 15, this indicates not only high energy transfer but also high momentum transfer. The mean scattering angle decreases as the energy of the incident neutrino increases, as shown in Fig. 16, meaning a more isotropic scenario. When E_ν approaches the target's chemical potential, we see a local peak in $\langle \theta \rangle$. More highly energetic neutrinos will on average scatter almost equally on any direction, resulting in small mean scattering angles.

D. Comparison with analytic approximations

When the matter is known to be completely degenerate, it is possible to find approximate expressions for the neutrino mean free paths with respect to the processes of absorption and of scattering, considering that the momenta of all matter constituents are fixed at their Fermi surface values. Neutrinos, on their turn, are considered to be either completely degenerate or nondegenerate.

For the absorption of degenerate neutrinos, it is found [15, 22]

$$\frac{1}{\lambda_a^D} = \frac{4G_F^2}{\pi^3} \cos^2 \theta_c \frac{p_{F_u}^2 p_{F_e}^3}{\mu_\nu^2} [(E_\nu - \mu_\nu)^2 + (\pi T)^2] \times \left[1 + \frac{1}{2} \frac{p_{F_e}}{p_{F_u}} + \frac{1}{10} \left(\frac{p_{F_e}}{p_{F_u}} \right)^2 \right], \quad (28)$$

where p_{F_i} is the Fermi momentum of particle species i . Eq. (28) is suitable for the case $|p_{F_u} - p_{F_e}| \geq |p_{F_d} - \mu_\nu|$. In the opposite situation, i.e., when $|p_{F_u} - p_{F_e}| \leq |p_{F_d} - \mu_\nu|$, the appropriate mean free path is obtained through the replacements $p_{F_u} \rightarrow p_{F_d}$ and $p_{F_e} \rightarrow \mu_\nu$. For the

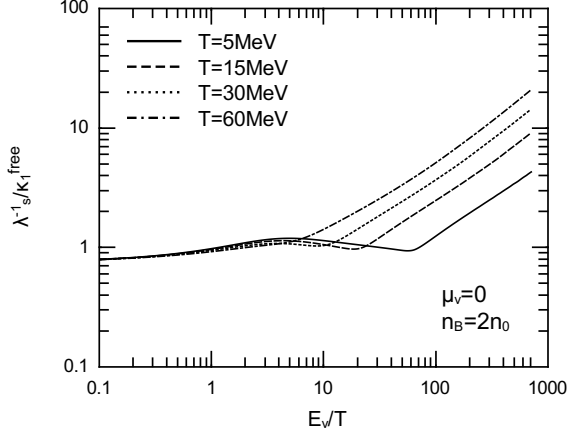


FIG. 12. Ratio between $1/\lambda_s$ given by Eq. (11) and κ_1 , Eq. (9), with the limiting approximation $f_1(E_\nu) \propto f_0(E_\nu)$ for nondegenerate neutrinos ($\mu_\nu = 0$).

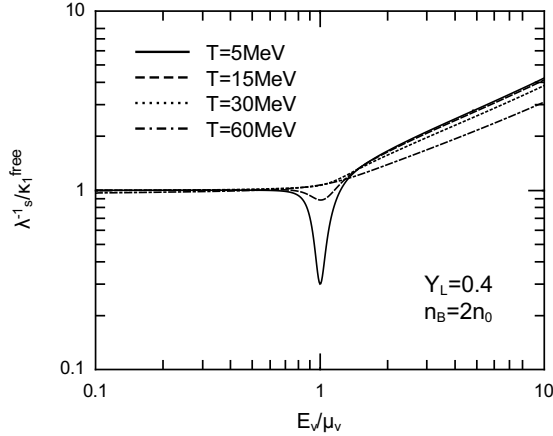


FIG. 13. The same as Fig. 12 but for degenerate neutrinos ($Y_L = 0.4$).

absorption of nondegenerate neutrinos, it is found

$$\frac{1}{\lambda_{a,ND}^D} = \frac{16}{\pi^4} \alpha_c G_F^2 \cos^2 \theta_c p_{F_u} p_{F_d} p_{F_e} \frac{E_\nu^2 + (\pi T)^2}{1 + e^{-E_\nu/T}} \quad (29)$$

The strong coupling constant, α_c , makes its appearance in Eq. (29) through the lowest-order corrections to the quarks' chemical potentials due to quark-gluon strong interaction

$$\mu_i = \left(1 + \frac{8}{3\pi} \alpha_c\right) p_{F_i}, \quad (30)$$

necessary to make the reaction kinematically allowed, since the masses of the u and d quarks are small and the neutrino momentum is not expected to play any significant role in the momentum conservation when they are nondegenerate, and hence, excluded from the momentum-conservation delta function [15].

The influence of the neutrino state of degeneracy on neutrino-electron scattering has been analyzed to great

extent. The inverse neutrino mean free path for degenerate neutrinos for this process has been found to be approximately [15, 30, 31]

$$\frac{1}{\lambda_s^D} = \frac{n_i \sigma_0}{20 m_e^2} [(E_\nu - \mu_\nu)^2 + (\pi T)^2] \sqrt{\frac{\mu_\nu}{p_{F_e}}} x_e \times [(C_{V,e}^2 + C_{A,e}^2)(10 + x_e^2) + 10 C_{V,e} C_{A,e} x_e], \quad (31)$$

for $E_\nu \gg T$. Here, $\sigma_0 = 4 G_F^2 m_e^2 \hbar^2 / \pi c^2 \simeq 1.74 \times 10^{-44} \text{ cm}^2$ and $x_e = \min(\mu_\nu, p_{F_e}) / \max(\mu_\nu, p_{F_e})$.

Approximate expressions for neutrino-electron scattering for nondegenerate neutrinos were found for different neutrino energy regimes [23]

$$\frac{1}{\lambda_s^{ND}} = [C_{V,e}^2 + C_{A,e}^2 + C_{V,e} C_{A,e}] \frac{n_e \sigma_0}{6 m_e^2} E_\nu p_{F_e} \quad (32)$$

for $E_\nu \gg p_{F_i}$, and

$$\frac{1}{\lambda_s^{ND}} = [C_{V,e}^2 + C_{A,e}^2] \frac{n_i \sigma_0}{40 m_e^2} \frac{E_\nu^3}{p_{F_e}}, \quad (33)$$

for $E_\nu \ll p_{F_e}$.

Neglecting the quark masses, the same results of Eqs. (31)-(33) are expected to be valid for neutrino-quark scattering, with appropriate coupling constants. It is important to note that in all of Eqs. (28)-(33) it is assumed that also electrons are completely degenerate. Tubbs & Schramm show approximations for neutrino-electron scattering when both neutrinos and electrons are nondegenerate [23].

In Fig. 18 we show a comparison between full numeric results and analytic approximations of Eqs. (28) and (29) for the process $\nu_e + d \rightarrow e^- + \nu_e$. In the case of degenerate neutrinos, we have divided the numeric results by the factor $1 - f_0(E_\nu)$, already included in the analytic results. In the nondegenerate case, we have used $\alpha_c = 0.1$ in Eq. (29) (with $\alpha_c = 0$ in the thermodynamic potential of quark matter). Larger values for α_c may result in better agreement with the numeric results for $E_\nu \gg T$ for this particular combination of temperature and density, but the same value for the strong coupling constant will not always give the better results for higher temperatures or densities for a given bag constant.

Using Eq. (29) requires then fixing α_c to an optimal value, whenever this is physically acceptable, so the approximation may give the best results in its domain of validity. Eq. (28), for absorption of degenerate neutrinos, on the other hand is shown to give good results only on the vicinity of $E_\nu = \mu_\nu$ and the results are better the higher the neutrino degeneracy is.

In the upper panels of Fig. 19 we compare the results given by Eqs. (32) and (33) with the numeric results for the indicated scattering processes of nondegenerate neutrinos. It is clear that the range of energies $E_\nu \lesssim T$ is in general not covered by the approximations. For the case of neutrino-electron scattering, Eq. (32) gives the better results for the whole range of energies, even though

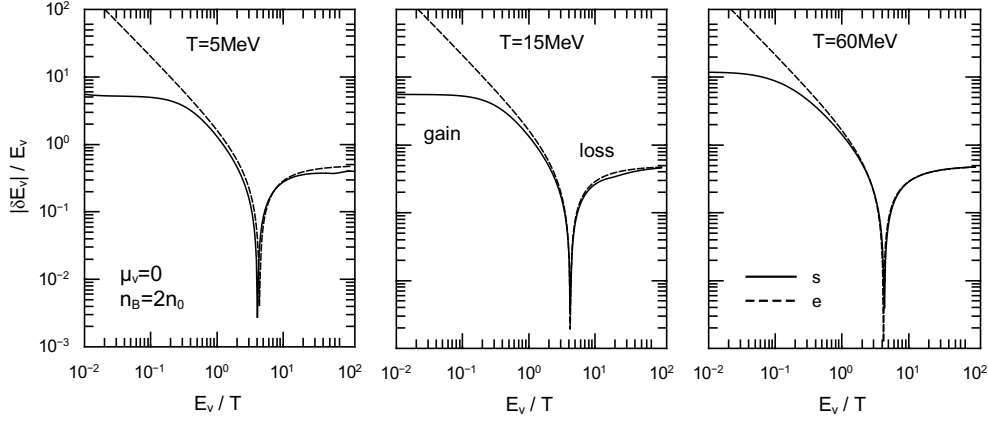


FIG. 14. Fractional mean energy transfer between nondegenerate neutrinos ($\mu_\nu = 0$) and matter at different temperatures. The energy transfer vanishes on average at $E_\nu \simeq 4T$.

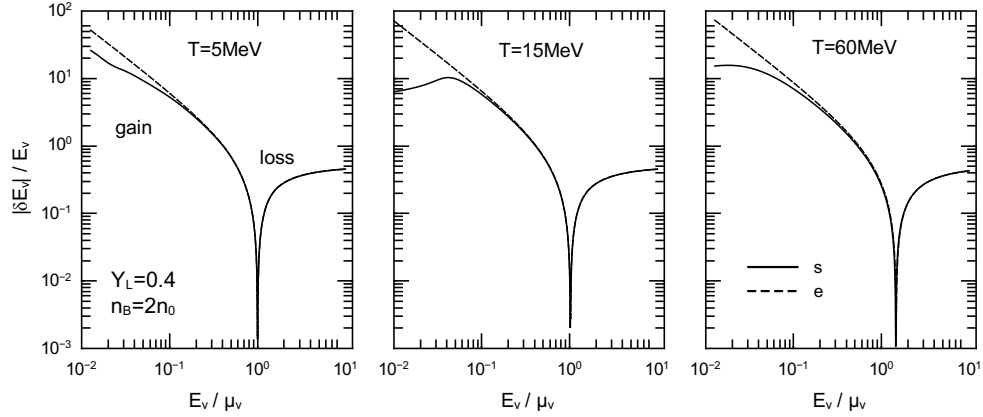


FIG. 15. Fractional mean energy transfer between degenerate neutrinos and quark matter at different temperatures. For very high degeneracy, the energy transfer vanishes on average at $E_\nu \simeq \mu_\nu$. For $T = 60\text{MeV}$, both neutrinos and quark matter are slightly less degenerate and the energy transfer vanishes on average at E_ν between μ_ν and $6T$. The curves associated with neutrino-up quark and neutrino-down quark scatterings are identical to the curves shown for neutrino-electron scattering and have thus been omitted.

its domain of validity is $E_\nu \gg p_{F_e}$. Nonetheless, it must be noticed that, in this case, results share only the same order of magnitude and, roughly, the same qualitative behavior.

In the lower panels of Fig. 19, we show how the results of Eq. (31) compare to the exact results. As in the case of absorption, the results are better for E_ν near μ_ν , nonetheless, the approximate results are in good qualitative agreement and same order of magnitude as the exact results also for $E_\nu < \mu_\nu$. In the panel of the middle, we show how the strange quark mass affects the scattering cross section.

Using the approximate mean free paths given by Eqs. (28)-(33), we calculate the neutrino Rosseland mean free path and compare the results against exact calculations. Since we considered only the cases of either highly degenerate or completely nondegenerate neutrinos, we did not use any interpolating procedure to join the different regimes, such as the one suggested by [32]. Also, it must

be noted that, for scatterings of nondegenerate neutrinos, only Eq. (33) was used. Even though an interpolating scheme to join smoothly Eqs. (32) and (33) can be proposed, this is not expected to improve the results too much, since this energy range is strongly cut-off by the factor $1/(1 - f_0(E_\nu))$.

The results shown in Fig. 20 reflect the fact that the approximations are, in general, good only on a limited range of neutrino energies. As one would expect, the analytic approximations of Eqs. (28)-(33) imply in generally poor agreement with exact results of energy-averaged opacities. Notoriously, the results are better for degenerate neutrinos. This can be understood from the fact that the approximations to the mean free paths tend to be better for neutrino energies near μ_ν and the integrands of Eq. (14) are highly weighted in the same region. Nevertheless, even in this case, the results agree only by order of magnitude and they share roughly the same qualitative behavior.

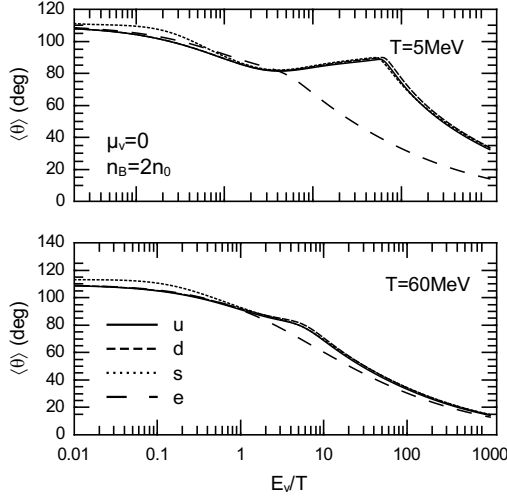


FIG. 16. Mean scattering angle $\langle\theta\rangle$ of nondegenerate neutrinos in quark matter. Here, u , d , s and e indicate the target particle.

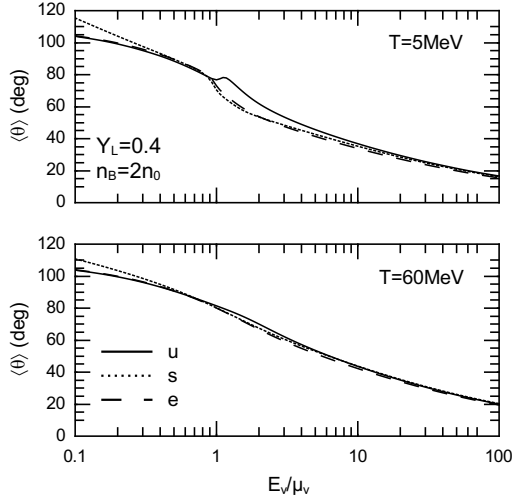


FIG. 17. The same as Fig. 16 but for $Y_L = 0.4$.

VI. SUMMARY AND CONCLUSIONS

We have analyzed in detail the neutrino mean free paths in quark matter. All the electron-neutrino weak interaction processes listed in Table I were considered. We have shown that, when neutrinos are nondegenerate, neutrino-quark scattering dominates the scattering contribution to the total neutrino opacity with respect to neutrino-electron scattering. On the other hand, when neutrinos are degenerate, the different scattering processes contribute almost the same, given that in this case, quark matter has a larger abundance of electrons.

In general, neutrino absorption constitutes the largest contribution to the neutrino opacity. However, neutrino scattering can represent a considerable fraction, amounting to about 40% in the highly leptonzonized scenario. When

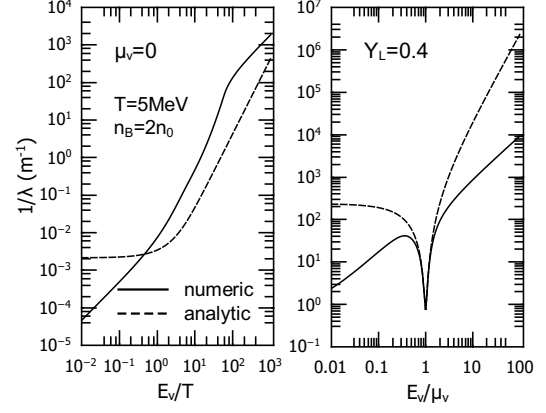


FIG. 18. Electron-neutrino inverse absorption mean free paths in quark matter at two times nuclear saturation density. Dashed lines indicate the approximations given in Eqs. (28) (right panel) and (29) (left panel).

neutrinos are nondegenerate, scattering represents no less than 10% of the total opacity, for temperatures in the range 5–60 MeV and baryon number density in the range $1 - 12n_0$.

We estimate that using $1/\lambda_s$, given in Eq. (9) instead of κ_1 given by Eq. (11) in the computation of the neutrino scattering mean free paths will represent an error of less than 10% in the total neutrino opacity. This upper bound is associated with the threshold of neutrino free-streaming, where f_1 is known to be proportional to f_0 and both $1/\lambda_s$ and κ_1 can be calculated and compared. In regions where neutrinos are closer to thermodynamic equilibrium, and f_1 is vanishingly small, this error is expected to be much smaller.

For baryon number densities in the range $1 - 12n_0$, the energy-averaged diffusion coefficients D_n , show a greater dependency on temperature than on density when T varies in the range 5–60 MeV. When neutrinos are nondegenerate, all of D_2 , D_3 and D_4 decrease with baryon density, while when neutrinos are degenerate they show different behaviors. In this case, D_2 decreases, while D_3 show no significant variation and D_4 increases with increasing density. We have also shown that the diffusion coefficients associated with antineutrinos are larger than those of neutrinos when the latter are nondegenerate. When neutrinos are degenerate, on the other hand, the diffusion coefficients of neutrinos are greater than those of antineutrinos.

Since we have not considered the presence of muons and taus in quark matter, the corresponding curves associated to the diffusion of muon and tau neutrinos have been left outside of the present work. Nevertheless, the following general remarks are worth addressing. Considering muon and tau neutrinos present in quark matter only in the form of thermally produced pairs, this type of neutrinos can take part only in the neutral-current scattering processes listed in Table I, given that the cor-

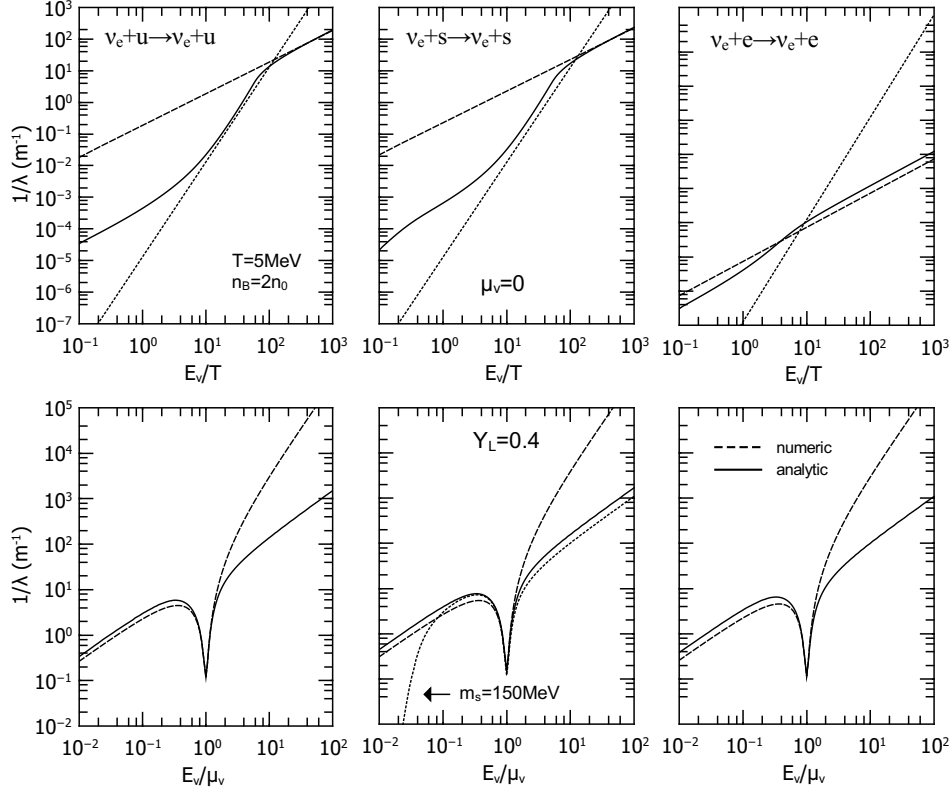


FIG. 19. Neutrino inverse scattering mean free paths. Upper panels: dashed lines indicate the approximations given in Eq. (32) and dotted lines are the results of Eq. (33). Lower panels: dashed lines indicate the results of Eq. (31). For comparison purposes, all quarks masses have been neglected in the numeric integrations. In the lower panel on the middle, the dotted line corresponds to the numeric result when $m_s = 150\text{MeV}$.

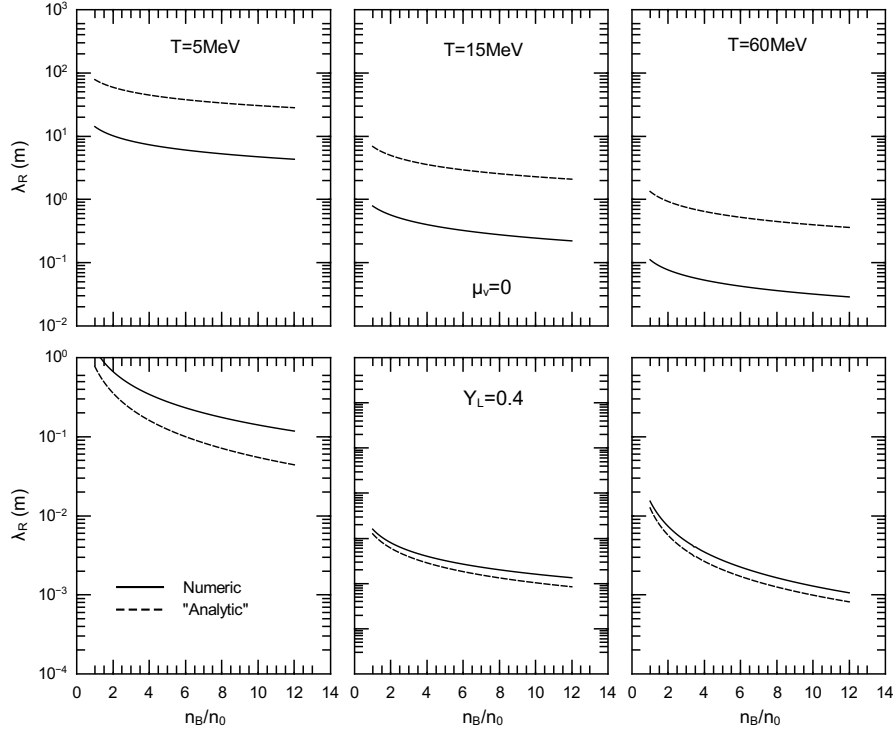


FIG. 20. Rosseland mean free paths for neutrinos in quark matter at different temperatures. “Analytic” results mean numeric integration over the incident neutrino energies using the energy-dependent approximations of Eqs. (28)-(33).

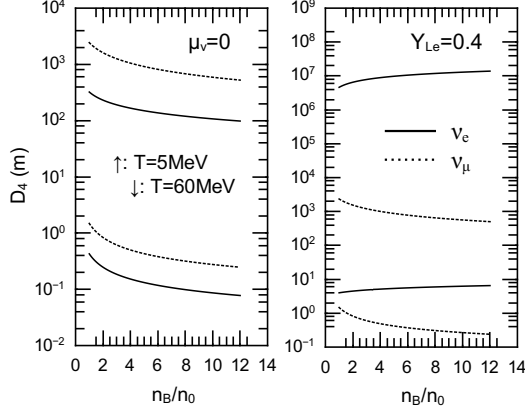


FIG. 21. Diffusion coefficient D_4 for electron neutrinos (full lines) and muon neutrinos (dashed lines). The topmost pairs of curves correspond to $T = 5\text{MeV}$ and those at the bottom correspond to $T = 60\text{MeV}$. Note that $\mu_\nu = 0$ and $Y_{Le} = 0.4$ correspond to electron neutrinos. Muon neutrinos always have $\mu_{\nu_\mu} = 0$ here.

responding charged-current processes are kinematically suppressed. It follows then that the total muon and tau neutrino mean free paths are generally increased in comparison with the total electron neutrino mean free paths. In particular, considering that the scattering opacity is the same for both muon and tau neutrinos, their contribution to the combined diffusion coefficient $D_4 = D_4^{\nu_e} + D_4^{\bar{\nu}_e} + 4D_4^{\nu_\mu}$ makes explicit their role in the energy transport in neutron stars, mainly in the regime of nondegenerate electron neutrinos, as we show in Fig. 21.

The influence of free parameters of the MIT bag model on the neutrino mean free paths have been analyzed. It is verified that increases in B , and α_c lead to increases in the total neutrino opacity, while a higher m_s decreases it. In general, when neutrinos are nondegenerate, increasing B from $60\text{MeV}/\text{fm}^3$ to $200\text{MeV}/\text{fm}^3$ or increasing m_s from 0 to 150MeV will affect more the neutrino opacity than does increasing α_c from 0 to 0.6 in the approximation of massless quarks. The same occurs when neutrinos are degenerate, with the difference that the effects are less prominent.

It should be noted that we have not considered here how many-body interactions may alter the neutrino cross-sections through correlations or collective behavior in general. In specific, we have neglected the possibility of quark pairing and color superconductivity and how the neutrino mean free paths are altered by it. In fact, at asymptotically high densities it has been shown from first principles that color superconductivity occurs in QCD. However, in the density regime relevant for neutron star physics such weak-coupling calculations are unreliable and most conclusions are obtained from phenomenological models that are claimed to capture the es-

sential physics of QCD. As a consequence, the actual occurrence of color superconductivity inside neutron stars is still an open question. Nevertheless, it is important to examine the impact of color superconductivity on the neutrino mean free paths and in fact this has been addressed in several works. For more details on the subject, we refer the reader to Refs. [37–42].

For last, neutrino-quark scattering share remarkable similarities with neutrino-electron scattering in what comes to neutrino/matter energy transfer and mean scattering angles. The general scenario is: low-energetic neutrinos tend to gain large amounts of energy and to scatter by larger angles. On the other hand, high-energetic neutrinos will lose on average half their initial energy and scatter almost isotropically.

ACKNOWLEDGMENTS

We would like to thank FAPESP and Universidade Federal do ABC for the financial support.

Appendix A: Neutrino inverse mean free path

With W_{fi} given in Eq. (17), Eq. (3) can be cast into several different forms for integration. To calculate the absorption mean free paths and the scattering mean free paths as in Eq. (11) it is convenient to use the total momentum as an integration variable. With that, all angular integrations can be performed and it only remains a double integration to be performed numerically [15, 18, 33, 34]:

$$\frac{1}{\lambda} = \frac{gG_F^2}{32\pi^5} E_\nu^{-2} \int_{m_2}^{\infty} dE_2 \int_{m_3}^{\infty} dE_3 E_3 \mathcal{S} [(C_V + C_A)^2 I_a + (C_V - C_A)^2 I_b - (C_V^2 - C_A^2) I_c], \quad (\text{A1})$$

where $\mathcal{S} = f_0(E_2)[1 - f_0(E_3)][1 - f_0(E_1 + E_2 - E_3)]$ and the integrals I_a , I_b and I_c are given by

$$I_a = \frac{\pi^2}{15} [3(P_{\max}^5 - P_{\min}^5) - 10(k_+^{\nu_2} + k_+^{\nu_3})(P_{\max}^3 - P_{\min}^3) + 60k_+^{\nu_2} k_+^{\nu_3} (P_{\max} - P_{\min})], \quad (\text{A2})$$

$$I_b = I_a(E_2 \leftrightarrow -E_3), \quad (\text{A3})$$

$$I_c = \frac{2\pi^2}{3} m_2 m_3 [(Q_{\max}^3 - Q_{\min}^3) + 6k_-^{\nu_3} (Q_{\max} - Q_{\min})], \quad (\text{A4})$$

with

$$k_{\pm}^{ij} = E_i E_j \pm 0.5 (p_i^2 + p_j^2), \quad (\text{A5})$$

$$P_{\min} = \max(|E_{\nu} - p_2|, |p_3 - p_4|), \quad (\text{A6})$$

$$P_{\max} = \min(E_{\nu} + p_2, p_3 + p_4), \quad (\text{A7})$$

$$Q_{\min} = |E_{\nu} - p_4|, \quad (\text{A8})$$

$$Q_{\max} = \min(E_{\nu} + p_4, p_2 + p_3). \quad (\text{A9})$$

Here, $p_4 = \sqrt{E_4^2 - m_4^2}$ and the particle labels follow the convention of Table I.

Appendix B: Scattering Kernels

We define the neutrino scattering kernels R^{out} as

$$R^{out} = g \int \frac{d^3 p_2}{(2\pi)^3} \int \frac{d^3 p_3}{(2\pi)^3} f(E_2)[1 - f(E_3)] W_{fi}, \quad (\text{B1})$$

where g denotes the total phase-space degeneracy factor and the integrations involve only the target particles. With W_{fi} given in Eq. (17), all integrations except one can be performed exactly. The results can be found in references [35, 36] (with the remark that our definition of R^{out} does not carry the overall $E_{\nu}^{\prime 2}$):

$$R^{out} = \int_{E_{min}}^{\infty} dE_2 \mathcal{S}'(E_{\nu} + E_2 - E'_{\nu}) [(C_V + C_A)^2 h_a + (C_V - C_A)^2 h_b - (C_V^2 - C_A^2) h_c], \quad (\text{B2})$$

where $\mathcal{S}' = f(E_2)[1 - f(E_{\nu} + E_2 - E'_{\nu})]$ and the integrals h_a , h_c and h_b are given by

$$h_a = \frac{g G_F^2}{(2\pi) E_{\nu} E'_{\nu}} [A E_2^2 + B E_2 + C], \quad (\text{B3})$$

$$h_b = h_a(E_{\nu} \leftrightarrow -E'_{\nu}), \quad (\text{B4})$$

$$h_c = \frac{g G_F^2}{(2\pi) E_{\nu} E'_{\nu}} \frac{m_2^2 E_{\nu} E'_{\nu} (1 - \cos \theta)}{\alpha^{1/2}}, \quad (\text{B5})$$

where $\alpha = E_{\nu}^2 + E_{\nu}^{\prime 2} - 2 E_{\nu} E'_{\nu} \cos \theta$, θ is the scattering angle. The quantities A , B and C are given by

$$A = \frac{\gamma^2}{\alpha^{5/2}} [E_{\nu}^2 + E_{\nu}^{\prime 2} + (3 + \cos \theta) E_{\nu} E'_{\nu}], \quad (\text{B6})$$

$$B = \frac{\gamma^2}{\alpha^{5/2}} E_{\nu} [2 E_{\nu}^2 + (3 - \cos \theta) E_{\nu} E'_{\nu} - (1 + 3 \cos \theta) E_{\nu}^{\prime 2}], \quad (\text{B7})$$

$$C = \frac{\gamma^2}{\alpha^{5/2}} E_{\nu}^2 \left[(E_{\nu} - E'_{\nu} \cos \theta)^2 - \frac{E_{\nu}^{\prime 2} \sin^2 \theta}{2} - \frac{m_2^2 (1 + \cos \theta)}{2 E_{\nu}^2 (1 - \cos \theta)} \alpha \right], \quad (\text{B8})$$

where we have also defined $\gamma = E_{\nu} E'_{\nu} (1 - \cos \theta)$. The lower integration limit in Eq. (B2), is given by

$$E_{min} = \frac{E'_{\nu} - E_{\nu}}{2} + \frac{\alpha^{1/2}}{2} \sqrt{1 + \frac{2m_2^2}{\gamma}}. \quad (\text{B9})$$

Appendix C: Mean energy transfer per scattering and mean scattering angle

From Fermi's golden rule, the neutrino interaction cross section can be written in terms of the squared matrix element, summed over final spins and averaged over the initial spins

$$\sigma = \frac{(2\pi)^{-6}}{4(p_{\nu} \cdot p_2)} \int \frac{d^3 p_3}{2E_3} \int \frac{d^3 p_4}{2E_4} \langle \mathcal{M} \rangle^2 \times (2\pi)^4 \delta(p_{\nu} + p_2 - p_3 - p_4), \quad (\text{C1})$$

for interactions happening on the vacuum. In thermodynamic systems, the particles involved in such scattering reactions have specific energy distributions and we must average the cross sections over their distribution functions and the availability of the initial and final states. In this case, we write

$$\bar{\sigma} = (2\pi)^{-5} g \int \frac{d^3 p_2}{2E_2} \int \frac{d^3 p_3}{2E_3} \int \frac{d^3 p_4}{2E_4} f_0(E_2)[1 - f_0(E_3)] \times [1 - f_0(E_4)] \frac{\langle \mathcal{M} \rangle^2}{4(p_{\nu} \cdot p_2)} \delta(p_{\nu} + p_2 - p_3 - p_4). \quad (\text{C2})$$

We define the mean energy transfer per collision between neutrinos and matter and the mean scattering angle as the averages

$$\delta E_{\nu} = \frac{g(2\pi)^{-3}}{\bar{\sigma}} \int \frac{d^3 p_2}{2E_2} \int dE'_{\nu} \mathcal{S}(E_{\nu} - E'_{\nu}) \left(\frac{\partial \sigma}{\partial E'_{\nu}} \right), \quad (\text{C3})$$

and

$$\langle 1 - \cos \theta \rangle = \frac{g(2\pi)^{-3}}{\bar{\sigma}} \int \frac{d^3 p_2}{2E_2} \int dE'_{\nu} \mathcal{S} \times \int d \cos \theta (1 - \cos \theta) \left(\frac{\partial^2 \sigma}{\partial E'_{\nu} \partial \cos \theta} \right), \quad (\text{C4})$$

where we have defined

$$\mathcal{S} = f_0(E_2)[1 - f_0(E_{\nu} + E_2 - E'_{\nu})][1 - f_0(E'_{\nu})]. \quad (\text{C5})$$

Note that we have added the blocking factor $1 - f_0(E'_{\nu})$, to account for neutrino degeneracy, in contrast to the results of [23]. Also, our definition of $\bar{\sigma}$ is only a shorthand for the quantity defined in Eq. (C2) and not a properly averaged statistical cross section as the one found in the same reference. For convenience, we have added a minus

overall sign in Eq. (C3) for the mere fact that we want negative values to represent energy loss.

Substituting $\langle \mathcal{M} \rangle^2$ on Eqs. (C3) and (C4), we obtain Eqs. of the form

$$\delta E_\nu = \frac{1}{\bar{\sigma}} [(C_V + C_A)^2 W_1 + (C_V - C_A)^2 W_2 + (C_A^2 - C_V^2) W_3] \quad (\text{C6})$$

and

$$\langle 1 - \cos \theta \rangle = \frac{1}{\bar{\sigma}} [(C_V + C_A)^2 U_1 + (C_V - C_A)^2 U_2 + (C_A^2 - C_V^2) U_3] \quad (\text{C7})$$

with the W s and U s given by Eqs. (21a)-(22c) of [23] with the inclusion of $[1 - f_0(\omega + \epsilon - \epsilon')]$ in all ϵ' integrations of the cited reference.

We would like to point slightly different definitions for δE_ν and $\langle 1 - \cos \theta \rangle$ that may be derived directly from Eq. (11):

$$\delta E_\nu = -\lambda_s \int_0^\infty dE'_\nu (E_\nu - E'_\nu) \left[\frac{\partial(1/\lambda_s)}{\partial E'_\nu} \right], \quad (\text{C8})$$

and

$$\langle 1 - \cos \theta \rangle = \lambda_s \int dE'_\nu \int d \cos \theta \times (1 - \cos \theta) \left[\frac{\partial^2(1/\lambda_s)}{\partial E'_\nu \partial \cos \theta} \right]. \quad (\text{C9})$$

Eq. (C9) can then be written in terms of the Legendre moments of the scattering kernel R^{out} :

$$\langle 1 - \cos \theta \rangle = 1 - \frac{\lambda_s}{(2\pi)^2} \int dE'_\nu E'^2_\nu [1 - f_0(E'_\nu)] R^{out}_1. \quad (\text{C10})$$

Even though Eqs. (C8) and (C10) differ from Eqs. (C3) and (C4) by the lack of the factor $(p_\nu \cdot p_2)^{-1}$ on the integrands (coming from the definition of cross section), they give fairly similar results and they can be more easily evaluated when R^{out} is available.

Appendix D: Analytic approximation to the diffusion D_n coefficients for degenerate neutrinos

In the case of highly degenerate neutrinos, the analytic approximations to the neutrino mean free paths with respect to both the neutral and charged currents, Eqs. (28)-(31), can be combined in the form

$$\frac{1}{\lambda_T} = \left[(x - \eta_\nu)^2 + \pi^2 \right] \frac{1}{g(\eta_\nu)}, \quad (\text{D1})$$

where

$$\frac{1}{g(\eta_\nu)} = \frac{1}{\eta_\nu^2} (a + b\eta_\nu^3 + c\eta_\nu^4 + d\eta_\nu^5) \quad (\text{D2})$$

with the coefficients given by

$$a = \left[\frac{G_F^2 T^5}{3\pi^3 (c\hbar)^7} \right] 12 \cos^2 \theta_c \eta_u^2 \eta_e^3 \left[1 + \frac{1}{2} \frac{\eta_e}{\eta_u} + \frac{1}{10} \left(\frac{\eta_e}{\eta_u} \right)^2 \right], \quad (\text{D3})$$

$$b = \left[\frac{G_F^2 T^5}{3\pi^3 (c\hbar)^7} \right] \sum_{i=u,d,s,e} g_i (C_{V,i}^2 + C_{A,i}^2) \eta_i^2, \quad (\text{D4})$$

$$c = \left[\frac{G_F^2 T^5}{3\pi^3 (c\hbar)^7} \right] \sum_{i=u,d,s,e} g_i C_{V,i} C_{A,i} \eta_i, \quad (\text{D5})$$

$$d = \left[\frac{G_F^2 T^5}{3\pi^3 (c\hbar)^7} \right] \frac{1}{10} \sum_{i=u,d,s,e} g_i (C_{V,i}^2 + C_{A,i}^2). \quad (\text{D6})$$

In these equations, $\eta_i = p_{F_i}/T$. Coefficients b to d are related only to the scattering reactions. Coefficient a has a counterpart as mentioned after Eq. (28), however, $|p_F(u) - p_F(e)| \geq |p_F(d) - \mu_\nu|$, tends to be the case when neutrinos are highly degenerate. Note also that we used $x_i = \mu_\nu/p_{F_i}$ in Eq. (31).

In this regime, the diffusion coefficients D_n read

$$D_n = g(\eta_\nu) \int_0^\infty dx x^n \left\{ \frac{f_0(E_\nu) [1 - f_0(E_\nu)]}{(x - \eta_\nu)^2 + \pi^2} \right\}. \quad (\text{D7})$$

The expression between curly braces can be approximated by

$$\frac{f_0(E_\nu) [1 - f_0(E_\nu)]}{(x - \eta_\nu)^2 + \pi^2} \simeq \frac{e^{-(x - \eta_\nu)^2/4}}{4\pi^2}, \quad (\text{D8})$$

and so Eq. (D7) can be solved by Gamma functions. One then arrives at

$$D_n = g(\eta_\nu) \frac{1}{4\pi^2} \sum_{k=0}^n \binom{n}{k} 4^{k/2} [1 + (-1)^k] \times \Gamma\left(\frac{k+1}{2}\right) \eta_\nu^{n-k}. \quad (\text{D9})$$

Explicitly:

$$D_2 = \frac{1}{2\pi^{3/2}} \left(\frac{2\eta_\nu^2 + \eta_\nu^4}{a + b\eta_\nu^3 + c\eta_\nu^4 + d\eta_\nu^5} \right), \quad (\text{D10})$$

$$D_3 = \frac{1}{2\pi^{3/2}} \left(\frac{6\eta_\nu^3 + \eta_\nu^5}{a + b\eta_\nu^3 + c\eta_\nu^4 + d\eta_\nu^5} \right), \quad (\text{D11})$$

$$D_4 = \frac{1}{2\pi^{3/2}} \left(\frac{12\eta_\nu^4 + 12\eta_\nu^4 + \eta_\nu^6}{a + b\eta_\nu^3 + c\eta_\nu^4 + d\eta_\nu^5} \right). \quad (\text{D12})$$

To perform a quick analysis, we assume, for simplicity, that $\eta_u \simeq \eta_d \simeq \eta_e \simeq \eta_\nu$ (which is, in fact, a reasonable assumption when neutrinos are highly degenerate). With this, the denominator on Eqs. (D10)-(D12) reduces to

$$a + b\eta_\nu^3 + c\eta_\nu^4 + d\eta_\nu^5 \simeq \left[\frac{G_F^2 T^5}{3\pi^3 (c\hbar)^7} \right] 19.78 \eta_\nu^5. \quad (\text{D13})$$

It is clear then that coefficients D_2 , D_3 and D_4 have

different behavior with respect to η_ν and, in particular, D_4 will increase with increasing neutrino degeneracy.

-
- [1] A. Bodmer, Phys. Rev. D **4**, 1601 (1971).
 - [2] H. Terazawa, INS Rep. 336, Univ. Tokyo, INS (1979).
 - [3] E. Witten, Phys. Rev. D **30**, 272 (1984).
 - [4] C. Alcock, E. Farhi, and A. Olinto, Astrophys. J. **310**, 261 (1986).
 - [5] P. Haensel, J.L. Zdunik, and R. Schaefer, Astron. Astrophys. **160**, 121 (1986).
 - [6] I. Bombaci, D. Logoteta, P. K. Panda, C. Providência, and I. Vidaña, Phys. Lett. B **680**, 448 (2009); G. Lugones and A. G. Grunfeld, Phys. Rev. D **84**, 85003 (2011); and references therein.
 - [7] F. Weber, *Pulsars as Astrophysical Laboratories for Nuclear and Particle Physics*, IOP Publishing Ltd. (1999).
 - [8] N. K. Glendenning, *Compact Stars: Nuclear Physics, Particle Physics, and General Relativity*, Springer (2000).
 - [9] P. Haensel, A. Y. Potekhin and D. G. Yakovlev, *Neutron Stars 1: Equation of State and Structure*, Springer (2007).
 - [10] G. Lugones, C. R. Ghezzi, E. M. de Gouveia Dal Pino, and J. E. Horvath, Astrophys. J. **581**, L101 (2002).
 - [11] P. Keranen, R. Ouyed, and P. Jaikumar, Astrophys. J. **618**, 485 (2005).
 - [12] B. Niebergal, R. Ouyed, and P. Jaikumar, Phys. Rev. C **82**, 062801 (2010).
 - [13] T. Fischer, I. Sagert, G. Pagliara, M. Hempel, J. Schaffner-Bielich, T. Rauscher, F. K. Thielemann, R. Käppeli, G. Martínez-Pinedo, and M. Liebendörfer, Astrophys. J. Supp. **194**, 39 (2011).
 - [14] G. Pagliara, M. Herzog, and F. K. Röpke, Phys. Rev. D **87**, 103007 (2013).
 - [15] N. Iwamoto, Annals of Physics **141**, 1 (1982).
 - [16] S. Reddy and M. Prakash, The Astrophysical Journal **478**, 689 (1997).
 - [17] S. Reddy, M. Prakash, and J. M. Lattimer, Physical Review D **58**, 013009 (1998).
 - [18] A. W. Steiner, M. Prakash, and J. M. Lattimer, Physics Letters B **509**, 10 (2001).
 - [19] S. W. Bruenn, The Astrophysical Journal Supplement Series **58**, 771 (1985).
 - [20] J. Cooperstein and E. Baron, The Astrophysical Journal **398**, 531 (1992).
 - [21] J. A. Pons, S. Reddy, M. Prakash, J. M. Lattimer, and J. A. Miralles, The Astrophysical Journal **513**, 780 (1999).
 - [22] R. F. Sawyer and A. Soni, The Astrophysical Journal **230**, 859 (1979).
 - [23] D. L. Tubbs and D. N. Schramm, The Astrophysical Journal **201**, 467 (1975).
 - [24] E. Farhi and R. Jaffe, Physical Review D **30**, 2379 (1984).
 - [25] J. I. Kapusta, Nuclear Physics B **148**, 461 (1979).
 - [26] O. Kalashnikov and V. Klimov, Physics Letters B **88**, 328 (1979).
 - [27] D. L. Tubbs, The Astrophysical Journal **231**, 846 (1979).
 - [28] D. L. Tubbs, The Astrophysical Journal Supplement Series **37**, 287 (1978).
 - [29] J. Bahcall, Physical Review **136**, 1164 (1964).
 - [30] D. Q. Lamb and C. J. Pethick, The Astrophysical Journal **209**, L77 (1976).
 - [31] B. T. Goodwin and C. J. Pethick, The Astrophysical Journal **253**, 816 (1982).
 - [32] W. Keil and H. Janka, Astronomy and Astrophysics **296**, 145 (1995).
 - [33] D. Shalitin, Astrophysics and Space Science **53**, 55 (1978).
 - [34] V. K. Gupta, A. Wadhwa, and J. D. Anand, Pramana **45**, 195 (1995).
 - [35] W. R. Yueh and J. R. Buchler, Astrophysics and Space Science **39**, 429 (1976).
 - [36] W. R. Yueh and J. R. Buchler, Astrophysics and Space Science **41**, 221 (1976).
 - [37] G. W. Carter and S. Reddy, Phys. Rev. D **62**, 103002 (2000).
 - [38] S. Reddy, M. Sadzikowski and M. Tachibana, Nucl. Phys. A **721**, 309 (2003).
 - [39] J. Kundu and S. Reddy, Phys. Rev. C **70**, 055803 (2004).
 - [40] T. Schäfer and K. Schwenzer, Phys. Rev. D **70**, 114037 (2004).
 - [41] P. Jaikumar, C. D. Roberts and A. Sedrakian, Phys. Rev. C **73**, 055803 (2006).
 - [42] K. Pal and A. K. Dutt-Mazumder, Phys. Rev. D **84**, 034004 (2011).